Peer-reviewed version available at *Geosciences* **2017**, *7*, 134; doi:10.3390/geosciences7040134

Article

Pyplis - A Python Software Toolbox for the Analysis of SO_2 Camera Data

Jonas Gliß [1,2,3]*, Kerstin Stebel [1], Arve Kylling [1], Anna Solvejg Dinger [1,4], Holger Sihler [5] and Aasmund Sudbø [3]

1 NILU - Norwegian Institute for Air Research, Kjeller, Norway
2 Department of Physics, University of Oslo (UiO), Oslo, Norway
3 Department of Technology Systems, University of Oslo (UiO), Kjeller, Norway
4 Institute of Environmental Physics (IUP), University of Heidelberg, Germany
5 Max Planck Institute for Chemistry (MPIC), Mainz, Germany
* Correspondence: jg@nilu.no; Tel.: +47-94885617

Version October 13, 2017 submitted to Entropy

Abstract: UV SO_2 cameras have become a common tool to measure and monitor SO_2-emission-rates, mostly from volcanoes but also from anthropogenic sources (e.g. power plants or ships). In the past years, the analysis of UV SO_2 camera data has seen many improvements. As a result, for many of the required analysis steps, several alternatives exist today. This inspired the development of *Pyplis*, an open-source software toolbox written in Python 2.7, which aims to unify the most prevalent methods from literature within a single, cross-platform analysis framework. *Pyplis* comprises a vast collection of algorithms relevant for the analysis of UV SO_2 camera data. These include several routines to retrieve plume background radiances as well as routines for cell and DOAS based camera calibration. The latter includes two independent methods to identify the DOAS field-of-view within the camera images. Plume velocities can be retrieved using an optical flow algorithm as well as signal cross-correlation. Furthermore, *Pyplis* includes a routine to perform a first order correction of the signal dilution effect. All required geometrical calculations are performed within a 3D model environment allowing for distance retrievals to plume and local terrain features on a pixel basis. SO_2-emission-rates can be retrieved simultaneously for an arbitrary number of plume intersections. *Pyplis* has been extensively and successfully tested using data from several field campaigns. Here, the main features are introduced using a dataset obtained at Mt. Etna, Italy on 16 September 2015.

Keywords: volcanic gases; SO_2; remote sensing; UV cameras; image processing; analysis software; Python 2.7

1. Introduction

Sulfur dioxide (SO_2) is a toxic gas emitted by anthropogenic and natural sources (e.g. power plants, ships, volcanoes). The pollutant has impacts on the atmosphere both on local and global scales (e.g. particle formation, radiation budget, e.g. [1], [2]). Furthermore, the monitoring of SO_2 emissions from active volcanoes can provide insight into the magma degassing behaviour and hence plays an important role for the development of new risk assessment approaches (e.g. [3], [4], [5], [6], and references therein).

The gas composition of the emission plumes can, inter alia, be studied using ground-based passive remote sensing techniques. The column-densities (CDs) of the gases in the plumes are quantified based on the absorption signature carried by scattered sunlight that has penetrated the plume. SO_2-CDs, for instance, can be retrieved at ultraviolet (UV) wavelengths (i.e. around 310 nm) where it exhibits distinct absorption bands. Prominent examples for passive remote sensing instrumentation are the correlation spectrometer (COSPEC, [7]), or instruments based on the DOAS technique (differential optical absorption spectroscopy, [8], e.g. [9], [10]). During the past years, the comparatively young technique of UV SO_2 cameras has gained in importance, since it enables to study volcanic SO_2 emissions

at unprecedented spatial and temporal resolution (e.g. [11], [12], [13], [14]). This is particularly helpful to study multiple sources independently (e.g. [15]) or to investigate volcanic degassing characteristics by studying periodicities in the SO_2-emission-rates (e.g. [16]). The technique of UV SO_2 cameras has seen remarkable improvements in the past years (e.g. [17], [18], [19], [20], [21]) and can nowadays be considered one of the standard methods for ground-based remote sensing of SO_2 plumes. A drawback, however, is the low spectral resolution, restricting the technique to a single species and furthermore, requiring external calibration.

The retrieval of SO_2-emission-rates from the plume imagery comprises several analysis steps which are summarised in Table 1 and are illustrated in the flowchart shown in the Appendix Figure A1. Thanks to ongoing developments, today, researchers can choose between several methods for nearly all of the required steps (e.g. cell vs. DOAS calibration, velocity retrieval using optical flow vs. cross-correlation method).

Available software solutions include Vulcamera ([22]), the IDL source code provided by [19] and Plumetrack ([23]). The first two programs include routines for cell calibration and cross-correlation based plume speed retrievals. The IDL program also includes a routine to perform a first order correction for the signal dilution effect. The software Plumetrack provides an interface to calculate gas velocities using an optical flow algorithm and can be applied to pre-calibrated SO_2-CD images in order to retrieve SO_2-emission-rates.

Table 1. Analysis blocks for emission-rate retrievals

Analysis block	Quantities	Analysis options	Sect.
Geometrical calculations	$\Delta s(m)$		3.1
Plume background analysis	τ_{on}, τ_{off}, τ_{AA}		3.3
Camera calibration	$S_{\text{SO2}}(m)$	Cell, DOAS	3.4
Plume speed retrieval	$\langle \vec{v}(m) \cdot \hat{\boldsymbol{n}}(m) \rangle$	Optical flow, cross-correlation	3.5
Emission-rate	Φ_{SO2}	Signal dilution correction	3.6, 3.7

Pyplis (***Py***thon ***pl***ume ***i***maging ***s***oftware) is a cross-platform, open-source software toolbox for the analysis of UV SO_2 camera data. The code is written in Python 2.7 and emerged from the idea of a common software platform incorporating the most relevant analysis methods, including recent developments. The most important features of *Pyplis* 0.13.4 are (details follow in Sect. 3):

1. 3D distance retrievals to plume and local terrain features at pixel-level,
2. several methods to retrieve plume background radiances,
3. cell and DOAS based camera calibration including two independent DOAS FOV search routines,
4. cross-correlation and optical flow based plume velocity retrievals,
5. histogram based correction for ill-posed optical flow vectors in low-contrast image regions,
6. image based correction for the signal dilution effect,
7. automated emission-rate retrievals along linear plume intersections.

Pyplis comes with numerous example scripts providing an easy and comprehensive introduction into the software. The following Sect. 2 introduces the technique of UV SO_2 cameras and the required analysis steps for SO_2-emission-rate retrievals. The implementation of the individual analysis methods is discussed in Sect. 3.

2. Methodology

2.1. UV SO_2 cameras

UV SO_2 cameras analyse scattered sun light which has penetrated a plume containing SO_2 gas. Plume optical densities (ODs) τ are retrieved in two wavelength windows of approximately 10 nm width, using optical bandpass filters. One filter is centred around 310 – 315 nm, where SO_2 has strong absorption bands (referred to as SO_2 on-band). A second filter is situated around 330 nm, where

Preprints (www.preprints.org) | NOT PEER-REVIEWED | Posted: 13 October 2017 doi:10.20944/preprints201710.0085.v1

Peer-reviewed version available at Geosciences 2017, 7, 134; doi:10.3390/geosciences7040134

SO_2 absorption is weak (SO_2 off-band). The latter is used to correct for additional broadband light extinction, for instance, resulting from aerosols or water droplets in the plume. From the retrieved ODs in both channels, the apparent absorbance (AA) of SO_2 (τ_{AA}, e.g. [17]) can be retrieved as

$$\tau_{AA} = \tau_{on} - \tau_{off} = \ln\left(\frac{I_0}{I}\right)_{on} - \ln\left(\frac{I_0}{I}\right)_{off}, \quad (1)$$

where I and I_0 denote the plume and plume background radiances, respectively, in both channels (on, off). Note that the method requires all additional optical densities in the on and off-band regime to be of broadband nature.

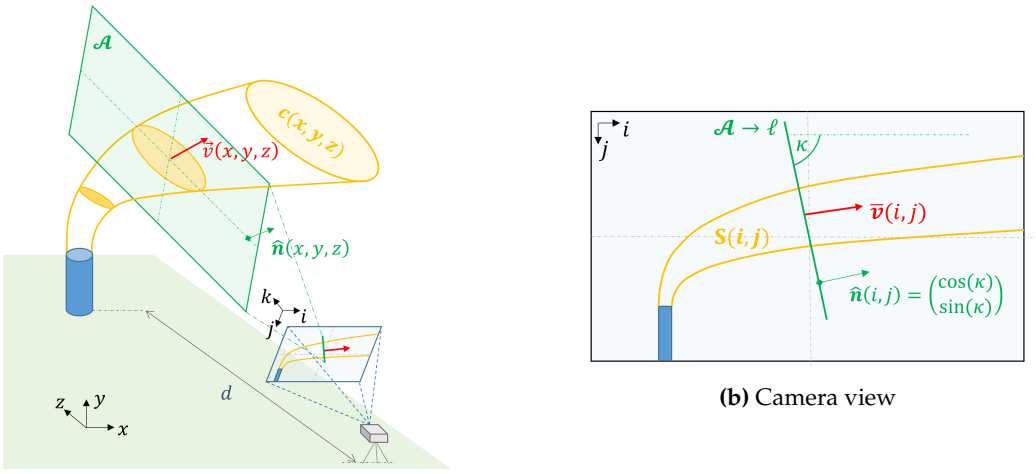

(a) 3D scene

(b) Camera view

Figure 1. Measurement geometry - sketched (a) in three dimensions and (b) as the camera sees it. The emission plume is indicated in yellow colours, gas velocities in red. The orientation of the plume cross-section (PCS) $\mathcal{A}$ (green colours) is aligned with the camera optical axis k.

2.2. Image analysis - Retrieval of S_{SO2} images

AA images are determined from a set of pre-processed (e.g. dark / offset corrected) plume and background images using Eq. 1. Next, the AA images are converted into SO_2 column-density (CD) images, where

$$S_{SO2}(i,j) = \int_{\mathcal{C}_{ij}} c(x,y,z)ds \quad (2)$$

denotes the SO_2-CD in the viewing direction $\mathcal{C}_{ij}$ of the image pixel i, j. $c(x,y,z)$ is the concentration distribution of SO_2 in real world coordinates x,y,z (cf. Figure 1a) and $ds = \sqrt{dx^2 + dy^2 + dz^2}$ is the integration differential.

The camera calibration (i.e. the conversion of AA values into SO_2-CDs) can be performed either using gas cells (e.g. [11]) or a co-located DOAS spectrometer (e.g. [18]). The latter is more accurate in case aerosols are present in the plume ([18], [24]). The position and shape of the DOAS FOV within the camera images is required in order to perform the DOAS calibration. The FOV can either be measured experimentally (e.g. in the lab) or can be retrieved directly from the field data ([18], [25]). The filter transmission curves shift towards lower wavelengths for non-perpendicular illumination. This leads to an increased SO_2 sensitivity towards the image edges. A correction for this effect can be performed during the image calibration using a sensitivity mask retrieved from cell calibration data (e.g. [18]).

Preprints (www.preprints.org) | NOT PEER-REVIEWED | Posted: 13 October 2017 doi:10.20944/preprints201710.0085.v1

Peer-reviewed version available at Geosciences 2017, 7, 134; doi:10.3390/geosciences7040134

2.3. Emission-rate retrieval

SO_2-emission-rates Φ are retrieved from SO_2-CD images by performing a discrete path integration along a suitable plume cross section (PCS) projected into the image plane, for instance a straight line $\boldsymbol{\ell}$ (illustrated in Figure 1b). Then,

$$\Phi(\boldsymbol{\ell}) = f^{-1} \sum_{m=1}^{M} S_{\mathrm{SO2}}(m) \cdot \langle \bar{\boldsymbol{v}}(m) \cdot \hat{\boldsymbol{n}}(m) \rangle \cdot d_{\mathrm{pl}}(m) \cdot \Delta s(m) \tag{3}$$

corresponds to the SO_2-emission-rate through $\boldsymbol{\ell}$, where m denotes one of a total of M sample positions along $\boldsymbol{\ell}$ in the image plane and Δs is the integration step length, measured in physical distances on the detector. f is the focal length of the camera, d_{pl} is the distance between camera and plume and $\hat{\boldsymbol{n}}$ is the normal of $\boldsymbol{\ell}$. $\bar{\boldsymbol{v}}$ is a 2-vector containing projected plume velocities averaged in the viewing direction.

The plume distances d_{pl} can be estimated from the measurement geometry and require information about the camera position and viewing direction as well as the source position and the meteorological wind direction. The gas velocities are usually retrieved from the images directly either using cross-correlation based methods (e.g. [26]) or optical flow algorithms (e.g. [20]).

Eq. 3 is equivalent to commonly used retrieval methods (e.g. [11], [24]) and is based on the assumption that over or underestimations of the measured quantities S_{SO2} and $\bar{\boldsymbol{v}}$ (e.g. due to non-perpendicular plume transects) cancel out in the emission-rate retrieval. This is a valid approximation for typical measurement conditions (i.e. plume nearly perpendicular to the optical axis, and plume extend small compared to plume distance). However, care has to be taken for unfavourable geometries (e.g. tilted or overhead plume; retrieval close to the image edges) which may require additional corrections (e.g. [27]).

If a locally uniform gas velocity can be assumed (i.e. $\bar{\boldsymbol{v}}(i,j) \rightarrow \bar{\boldsymbol{v}}$) and further, a planar PCS is used for the retrieval (i.e. $\hat{\boldsymbol{n}}(i,j) \rightarrow \hat{\boldsymbol{n}}$) then, Eq. 3 can be further approximated as $\Phi(\boldsymbol{\ell}) \approx \langle \bar{\boldsymbol{v}} \cdot \hat{\boldsymbol{n}} \rangle \cdot \chi(\boldsymbol{\ell})$, where

$$\chi(\boldsymbol{\ell}) = f^{-1} \sum_{m=1}^{M} S_{\mathrm{SO2}}(m) \cdot d_{\mathrm{pl}}(m) \cdot \Delta s(m) \tag{4}$$

denotes the integrated column amount (ICA) along $(\boldsymbol{\ell})$.

2.4. Radiative transfer corrections

Radiative transfer effects may introduce systematic errors in the retrieved emission-rates (see e.g. [28], [29]). The signal dilution effect describes a decrease in the measured CDs due to scattering between instrument and plume. The magnitude of this effect primarily depends on the local visibility (i.e. amount of molecules and particles in the ambient atmosphere) and on the distance between camera and plume. A first order correction can be performed using the atmospheric scattering extinction coefficients in the viewing direction between camera and source (e.g. [12], [30]). The latter can be retrieved, for instance, by studying brightness variations of topographic terrain features in the images as a function of their distance to the instrument ([19]). More complicated radiative transfer issues (e.g. optically thick plumes) require corrections using radiative transfer models (e.g. [24]). *Pyplis* can correct for the signal dilution effect based on the method suggested by [19].

3. Implementation

In the following, the main features and modules of *Pyplis* are presented. The API is designed modular using object oriented architecture. It can therefore be used in parts or as a whole. Figure 2 illustrates the *Pyplis* API for SO_2-emission-rate retrievals (see also Appendix D). *Pyplis* includes 19 example scripts, which provide an introduction into the main features of the software (summarised in Table A1). The scripts are based on an example dataset recorded at Mt. Etna in Italy on 16/09/2015

Preprints (www.preprints.org) | NOT PEER-REVIEWED | Posted: 13 October 2017 doi:10.20944/preprints201710.0085.v1

Peer-reviewed version available at Geosciences 2017, 7, 134; doi:10.3390/geosciences7040134

between 06:40 – 07:30 UTC. These data is freely available and can be downloaded from the website (for details see Appendix E.1).

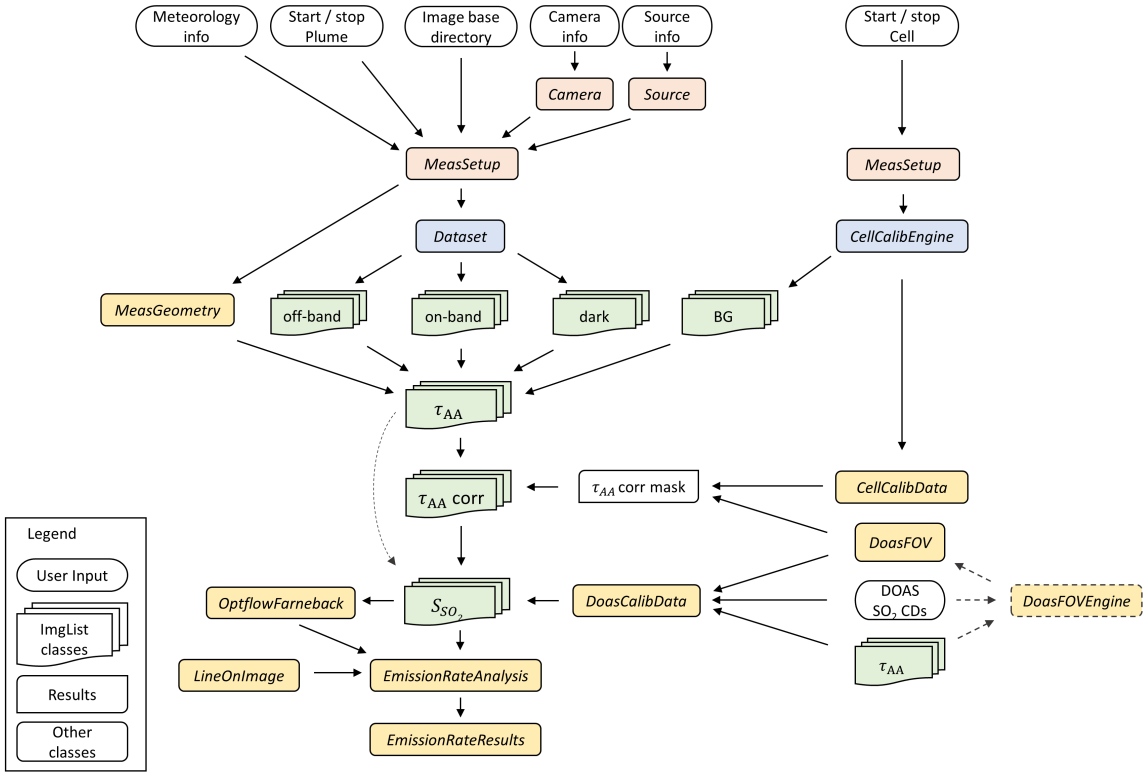

Figure 2. *Pyplis* API - Flowchart illustrating the main analysis steps and the corresponding classes of the *Pyplis* API for SO_2-emission-rate retrievals. *Italic* denotations correspond to class names in *Pyplis*. Optional analysis steps are indicated by dashed boxes. `Setup` classes (red) include relevant meta information and can be used to create `Dataset` objects (blue). The latter perform file separation by image type and create `ImgList` objects (green) for each type (e.g. on, off, dark). Further analysis classes are indicated in yellow. Note that the routine for signal dilution correction is not shown here (cf. Figure A1).

3.1. Geometrical calculations

Geometrical calculations are performed within an instance of the `MeasGeometry` class (part of the *geometry.py* module). The plume distances d_{pl} (cf. Eq. 3) can be retrieved per pixel-column i using intersections of the respective viewing azimuth with the plume azimuth (see Figure 3). This requires specification of the camera position, viewing direction and optics (e.g. detector specifications, focal length), source coordinates and meteorological wind direction. The distances are determined based on the horizontal plume distance and the altitude difference between source and camera (i.e. assuming a horizontally aligned plume). It is pointed out, that this approach may be inapplicable for complicated measurement geometries (e.g. overhead plumes), which would require a more detailed knowledge of the plume shape and altitude.

Further features of the `MeasGeometry` class include a routine to retrieve the camera viewing direction based on the position of distinct objects in the images (e.g. summit of volcano, cf. Figure 3), or the calculation of distances to topographic features in the images (shown in Figure 10, for details see Appendix A). Furthermore, 2D and 3D topographic overview maps of the measurement setup can

Preprints (www.preprints.org) | NOT PEER-REVIEWED | Posted: 13 October 2017 doi:10.20944/preprints201710.0085.v1

Peer-reviewed version available at Geosciences 2017, 7, 134; doi:10.3390/geosciences7040134

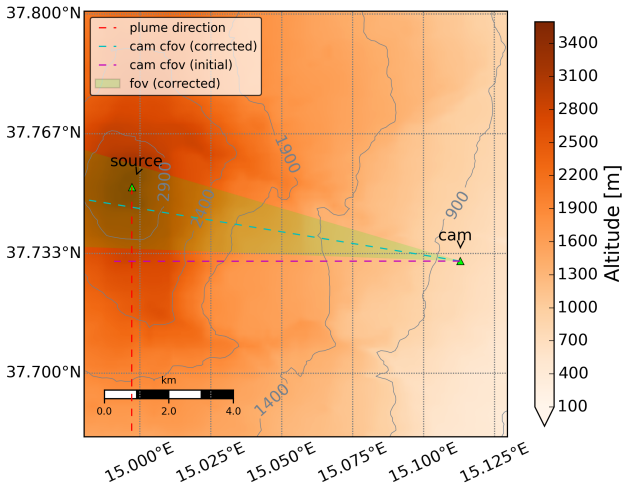

Figure 3. Measurement geometry - 2D overview map of the measurement setup at Mt. Etna from the *Pyplis* example data. The map includes plume orientation (red dashed line), camera azimuth retrieved using a compass (purple dashed line) and the corrected camera azimuth (blue dashed line) and corresponding FOV (semi-transparent green), retrieved automatically using the position i, j of the Etna south-east crater within the images and the corresponding coordinates of the crater (longitude, latitude, altitude). The map was generated using a `MeasGeometry` object (see Sect. 3.1).

be created automatically (as shown in Figure 3, see also Figure 10c). The `MeasGeometry` class uses the Python Geonum library ([31]) which is briefly introduced in Appendix A.

3.2. Image representation and pre-processing routines

Images are represented by the `Img` class (*image.py* module). The `Img` class includes reading routines for all image formats supported by the Python Imaging Library (PIL, e.g. png, tiff, jpeg, bmp) as well as the FITS format (Flexible Image Transport System). It further allows to store relevant meta information (e.g. exposure and acquisition time, focal length, f-number) and includes several basic processing methods (e.g. smoothing, cropping or resizing using a Gaussian pyramid approach). The image data itself is loaded and stored as a 2D-NumPy array within an `Img` object. Automatic dark and offset correction can be performed as described in Appendix B. `Img` objects can be saved as FITS files at any stage of the analysis (e.g. dark corrected image, τ_{AA} image, calibrated SO_2-CD image).

3.3. Retrieval of plume background radiances

The calculation of the OD images in both wavelength channels requires the retrieval of the sky-background intensities I_0 behind the plume (cf. Eq. 1). The *plumebackground.py* module provides several alternatives to retrieve the background intensities, either from the plume images directly or using an additional sky reference image (I_0-image). For the latter, several methods are available to correct for offsets and non-uniformities in the sky-background between the plume and I_0-image. The corrections are based on suitable sky-reference-areas in the plume image (rectangles or profile-lines, cf. Table 2) and use 1^{st} or 2^{nd} order polynomials to model the I_0-image such, that the corresponding OD image satisfies $\tau = 0$ within the specified sky reference areas.

If no I_0-image is available, the plume background radiances can also be estimated from the plume images directly using a masked 2D polynomial surface fit. The required mask specifies clear-sky image pixels which are considered during the fit. The mask can either be provided by the user or can be retrieved automatically using the method `find_sky_background`.

Preprints (www.preprints.org) | NOT PEER-REVIEWED | Posted: 13 October 2017 doi:10.20944/preprints201710.0085.v1

Peer-reviewed version available at Geosciences 2017, 7, 134; doi:10.3390/geosciences7040134

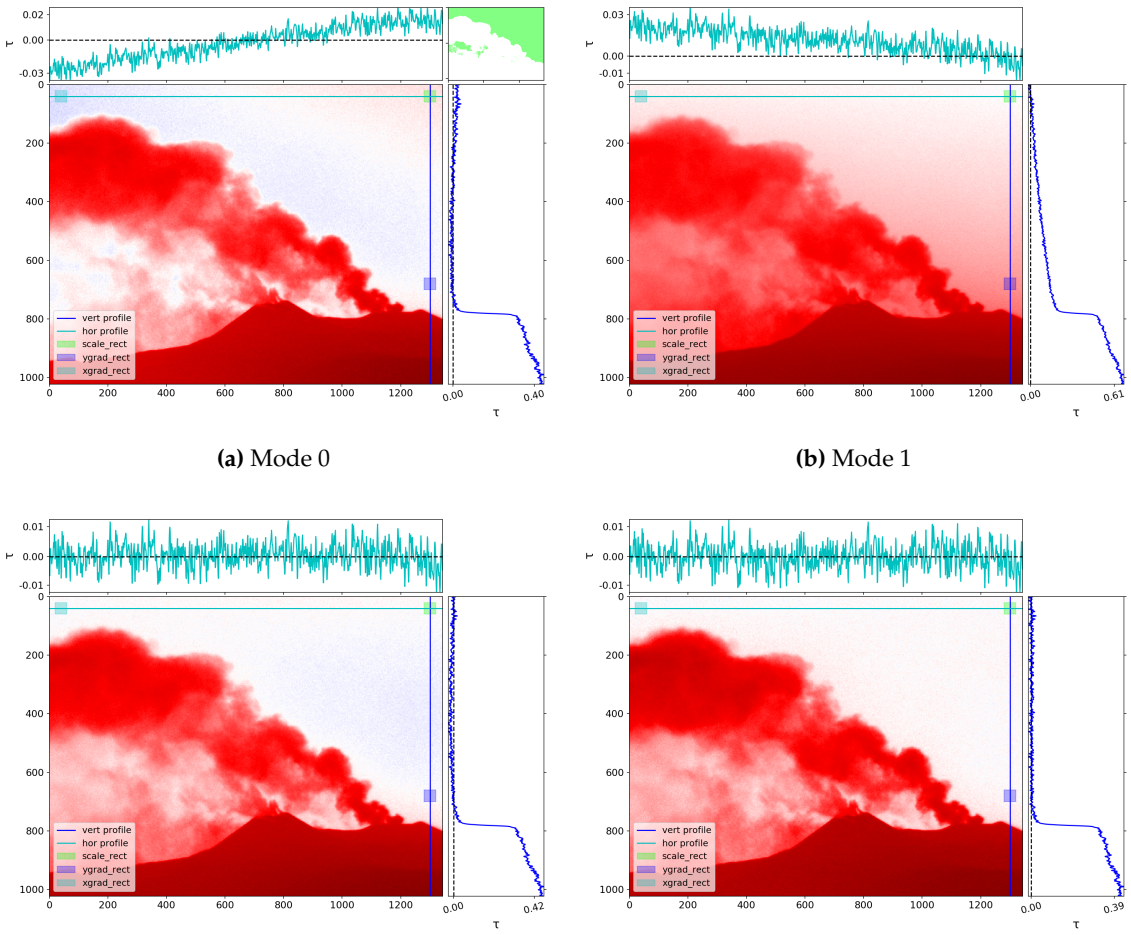

(a) Mode 0 **(b)** Mode 1

(c) Mode 4 **(d)** Mode 6

Figure 4. Plume background modelling - Four example on-band OD images (τ_{on}) determined using background modelling modes 0 (polynomial surface fit) and 1, 4 and 6 (based on I_0-image, cf. Table 2). Horizontal and vertical profiles are plotted on the top and on the right, respectively. The top-left plot (Mode 0) further includes the mask specifying sky-reference pixels (green area) which was used for the polynomial surface fit. The plume and background images used for the displayed examples were recorded at 07:06 UTC and at 07:02 UTC, respectively.

The `PlumeBackgroundModel` class (part of *plumebackground.py*) provides high level access to eight default methods for the background retrieval. The methods are summarised in Table 2. Figure 4 shows four example plume on-band OD images calculated using the modelling modes 0, 1, 4 and 6. It is not intended to give a recommendation for a "best" method here, as this strongly depends on the data (e.g. availability of suitable reference areas; acquisition time and relative viewing direction of I_0-image; solar position).

Preprints (www.preprints.org) | NOT PEER-REVIEWED | Posted: 13 October 2017 doi:10.20944/preprints201710.0085.v1

Peer-reviewed version available at Geosciences 2017, 7, 134; doi:10.3390/geosciences7040134

Table 2. Available plume background modelling modes of the `PlumeBackgroundModel` class (cf. names of sky reference areas in Figure 4)

		Corrections		
Mode	I_0**-img**	Scaling	Vertical	Horizontal
1	yes	scale_rect		
2	yes	scale_rect	ygrad_rect (linear)	
3	yes	scale_rect	vert. profile (quadratic)	
4	yes	scale_rect	ygrad_rect (linear)	xgrad_rect (linear)
5	yes	scale_rect	vert. profile(quadratic)	xgrad_rect (linear)
6	yes	scale_rect	vert. profile (quadratic)	hor. profile (quadratic)
0	no	Masked 2D polynomial surface fit		
99	yes	None (use I_0-img as is)		

3.4. Camera calibration

The camera calibration can either be performed using data based on cuvettes filled with a known amount of SO_2-gas, or using plume SO_2-CDs retrieved from a co-located DOAS spectrometer (cf. Table 1).

3.4.1. Calibration using SO_2 cells

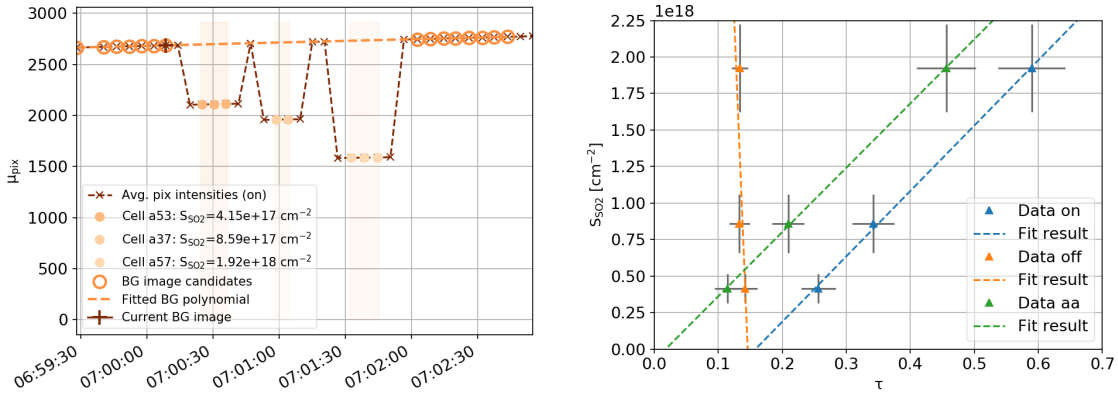

(a) Cell search result on-band

(b) Example calibration curves

Figure 5. Cell calibration - (a) shows the output of the automatic cell search routine (included in the `CellCalibEngine` class). (b) shows example calibration curves for τ_{on}, τ_{off} and τ_{AA} images for the image center pixel from the dataset shown in (a).

Cell calibration can be performed using the `CellCalibEngine` class (*cellcalib.py* module) and requires a dataset containing both cell and sky background images. It is assumed, that the camera is pointed into a gas and cloud free area of the sky and that the cells (containing different SO_2-CDs) are consecutively placed in front of the lens, such that they cover the whole FOV of the camera. Figure 5a shows a time-series of the image mean intensities retrieved from such a dataset. The individual cells can be identified by abrupt intensity drops in the time-series while the ambient background only changes gradually. The corresponding time-intervals for cell and background images can be specified by the user or alternatively, detected automatically within an instance of the `CellCalibEngine` class (shown in Figure 5a,see also ex. scripts 0.7 and 5).

Cell OD images in both channels (τ_{on}, τ_{off}) can be determined using a suitable background image. Care has to be taken for measurements performed at large solar zenith angles (early morning, late afternoon) due to rapid changes of the ambient sky intensity (cf. Figure 5a). In this case the background image

Preprints (www.preprints.org) | NOT PEER-REVIEWED | Posted: 13 October 2017 doi:10.20944/preprints201710.0085.v1

Peer-reviewed version available at Geosciences 2017, 7, 134; doi:10.3390/geosciences7040134

needs to be scaled to the sky intensity present at the acquisition time of each cell in order to calculate the OD images. This correction was performed for the data shown in Figure 5a (i.e. dashed line "Fitted BG polynomial"). It requires at least two background images, one recorded before, and a second one after the cells were put in front of the lens.

The calibration results (e.g. one AA image for each cell) are stored within `CellCalibData` objects together with the corresponding cell SO_2-CDs (which need to be provided by the user). Calibration curves can then be retrieved per image pixel or within a certain pixel neighbourhood. Figure 5b shows example calibration curves for τ_{on}, τ_{off} and τ_{AA} images.

3.4.2. Calibration using DOAS data

The DOAS calibration is performed using a set of plume optical density images (usually AA images) and a corresponding time-series of SO_2-CDs retrieved from a DOAS spectrometer[1]. In a first step, the AA images are stacked into a 3D-NumPy array and merged in time with the DOAS data. The latter can be performed in three different ways (for details see Appendix C.1). The calibration data (i.e. merged time-series of SO_2-CDs and camera AA values within the DOAS FOV) can be retrieved by convolving the AA stack with a mask specifying position and shape of the DOAS field-of-view (FOV) within the image plane. The calibration data is stored within instances of the `DoasCalibData` class, which is also used to retrieve the calibration curve. The latter is done by fitting a polynomial of appropriate order to the calibration data. Optionally, the fit can be performed using a weighted regression, to account for statistical uncertainties in the DOAS SO_2-CDs (e.g. fit-errors, cf. Figure 6). `DoasCalibData` objects can be stored using the FITS standard (including the FOV mask).

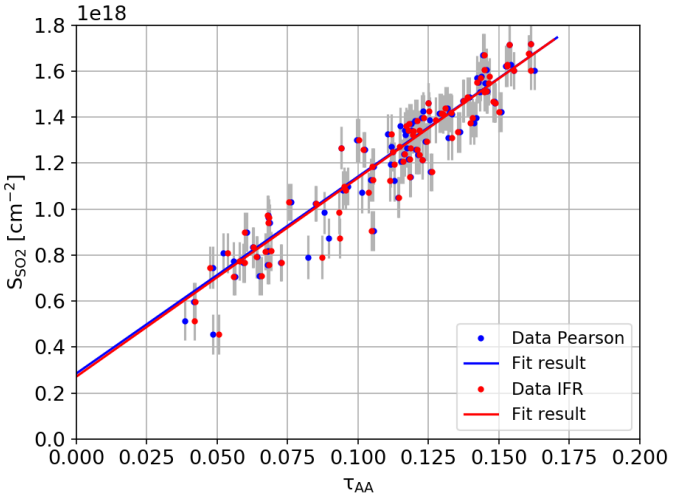

Figure 6. DOAS calibration curves - Plot showing example DOAS calibration data corresponding to the two different FOV parametrisations shown in Figure 7). The fit was performed using a first-order weighted polynomial fit. The weights where calculated using the relative errors ΔS_{SO2} / S_{SO2} of the DOAS SO_2-CDs. The y-axis offset is likely due to uncertainties in the DOAS retrieval (e.g. due to O_3 interference) and is compensated by the calibration.

[1] Note: *Pyplis* cannot perform the DOAS analysis, the SO_2-CDs need to be retrieved using suitable 3rd party software, e.g. DOASIS, [32]

Preprints (www.preprints.org) | NOT PEER-REVIEWED | Posted: 13 October 2017 doi:10.20944/preprints201710.0085.v1

Peer-reviewed version available at Geosciences 2017, 7, 134; doi:10.3390/geosciences7040134

Note that the DOAS calibration curve is only valid within the image pixel area covered by the DOAS FOV. This is due to cross-detector variations in the SO_2 sensitivity (see Sect. 2.2) and can be corrected for using a mask retrieved from a cell calibration dataset. The mask is determined by fitting a 2D polynomial to a cell AA image (see prev. Sect. 3.4.1) which is then normalised to the centre-position of the DOAS FOV (illustrated in ex. script 7).

3.4.3. DOAS FOV search

Pyplis includes two routines to retrieve the DOAS FOV mask (included in the `DoasFOVEngine` class) based on a stack of AA images and a DOAS data vector:

1. **Pearson routine**: this method loops over all image pixels in the AA stack and determines the Pearson correlation coefficient between the corresponding AA time-series ($\tau_{AA}(t)$) and the DOAS SO_2-CD vector ($S_{SO2}(t)$). The method yields a correlation image as shown in Figure 7a, from which the pixel coordinate with highest correlation (i_0, j_0) is extracted (see also [18]). Assuming a circular FOV shape, the pixel extend of the FOV is estimated around i_0, j_0, by iteratively searching the disk radius with highest correlation between the AA and the DOAS time-series.
2. **IFR routine**: this method is based on [25] and uses an inversion algorithm to retrieve the FOV. Position and shape of the FOV is parametrised by fitting a 2D Super-Gaussian to the retrieved FOV distribution (shown in Figure 7b, see Appendix C.2 for details).

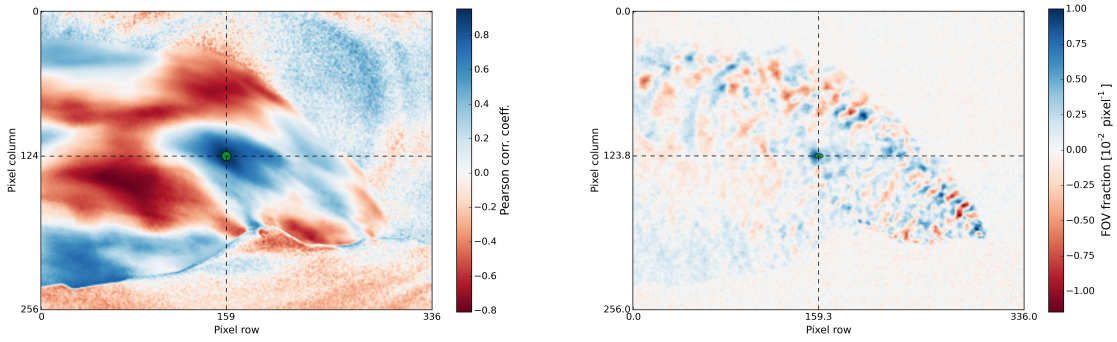

(a) Pearson method **(b)** IFR method

Figure 7. DOAS FOV search - DOAS FOV search results using (a), the *Pearson* and (b), the *IFR* method. The Pearson method (a) yields a FOV centered at $i = 159$, $j = 124$ and a disk radius of 4 pixels. For the IFR retrieval (b) a tolerance factor of $\lambda = 2 \cdot 10^{-3}$ was chosen and a Super-Gaussian (without tilt) was fitted to the correlation image yielding a FOV centered at $i = 159.3$, $j = 123.8$, $\sigma = 7.1$, asymmetry parameter $a = 1.9$ and a shape parameter of $b = 0.3$ (for details see Eq. A2). The retrieved FOV positions show good agreement. Note, that the FOV was retrieved from downscaled images (Gauss pyramid level 2).

The retrieved FOV information (position, shape, convolution mask) is represented by the `DoasFOV` class and can be stored as FITS file.

3.5. Plume velocity analysis

Plume velocities can be retrieved either using the ICA cross-correlation method or using an optical flow algorithm. Both methods yield displacement estimates in units of pixels / time. These are converted into plume gas velocities based on the measurement geometry (`MeasGeometry`, see Sect. 3.1). The relevant code is implemented in the *plumespeed.py* module.

Preprints (www.preprints.org) | NOT PEER-REVIEWED | Posted: 13 October 2017 doi:10.20944/preprints201710.0085.v1

Peer-reviewed version available at Geosciences 2017, 7, 134; doi:10.3390/geosciences7040134

3.5.1. Velocity retrieval using the ICA cross-correlation method

For the cross-correlation method, ICA time-series (see Eq. 4) are determined using two PCS lines located at different positions downwind the emission source. Ideally, the PCS lines should be parallel and should cover an entire plume cross-section (indicated in Figure 8, left). In a first step, the two time-series are re-sampled onto a regular grid (default is 1 s resolution). In a second step, a correlation analysis is applied to the re-sampled data vectors in order to find the time lag corresponding to the highest correlation between both signals[2]. The method yields one average velocity vector, which is representative for the used image region and time-series. Note that the method intrinsically assumes, that the average plume propagation direction $\bar{\varphi}$ in the i, j-plane is aligned with the PCS normal (i.e. $\bar{\varphi} \parallel \hat{\boldsymbol{n}}$). Figure 8 shows results from an example cross-correlation analysis, resulting in a plume velocity of 3.5 m/s.

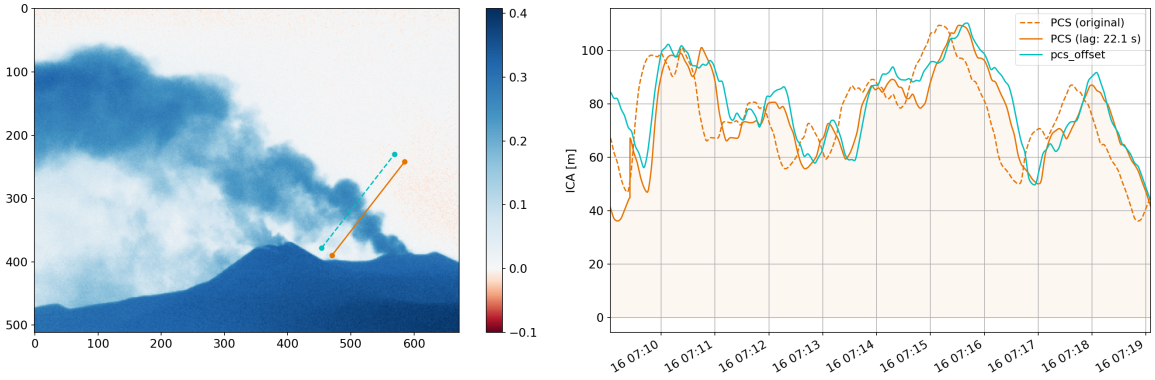

Figure 8. Plume velocity retrieval using cross-correlation method. Left: example on-band OD image and the two used PCS lines. Right: ICA time-series for both lines (orange dashed and cyan line) and the PCS signal shifted using the retrieved correlation lag of 22.1 s (orange profile). The analysis yields an average gas velocity of 3.5 m/s.

3.5.2. Optical flow based velocity retrievals

Optical flow velocity retrievals are performed using the Farnebäck algorithm ([33]) which is implemented in the OpenCV library ([34]). The algorithm can estimate motion at the pixel-level by tracking local contrast features between consecutive frames. Note, however, that optical flow algorithms may fail to detect motion in extended homogeneous image areas. In this case, appropriate corrections may be required (e.g. [35]).

All relevant calculations for optical flow based velocity retrievals are performed within the `OptflowFarneback` class. The class includes the Farnebäck algorithm itself as well as several pre and post-analysis routines. The latter include a routine that can detect and correct for unphysical motion estimates in homogeneous image regions based on the method proposed by [35]. The correction identifies the local average velocity vector using peaks in histograms of an optical flow motion field.

The Farnebäck algorithm itself requires specification of several input parameters (see e.g. OpenCV documentation). The *Pyplis* default settings follow the suggestions of [20]. An example flow field is shown in Figure 9 including results from the histogram post analysis within a narrow ROI around an example retrieval line. The latter yield an average velocity magnitude of 4.2 ($\pm$ 0.4) m/s and a predominant movement direction of $\varphi = -65\,(\pm 14)\,^\circ$ within the image plane. Optical flow plume

[2] Note that the cross-correlation method is based on the fundamental assumption, that SO_2 is conserved between the two PCS lines.

Preprints (www.preprints.org) | NOT PEER-REVIEWED | Posted: 13 October 2017 doi:10.20944/preprints201710.0085.v1

Peer-reviewed version available at Geosciences 2017, 7, 134; doi:10.3390/geosciences7040134

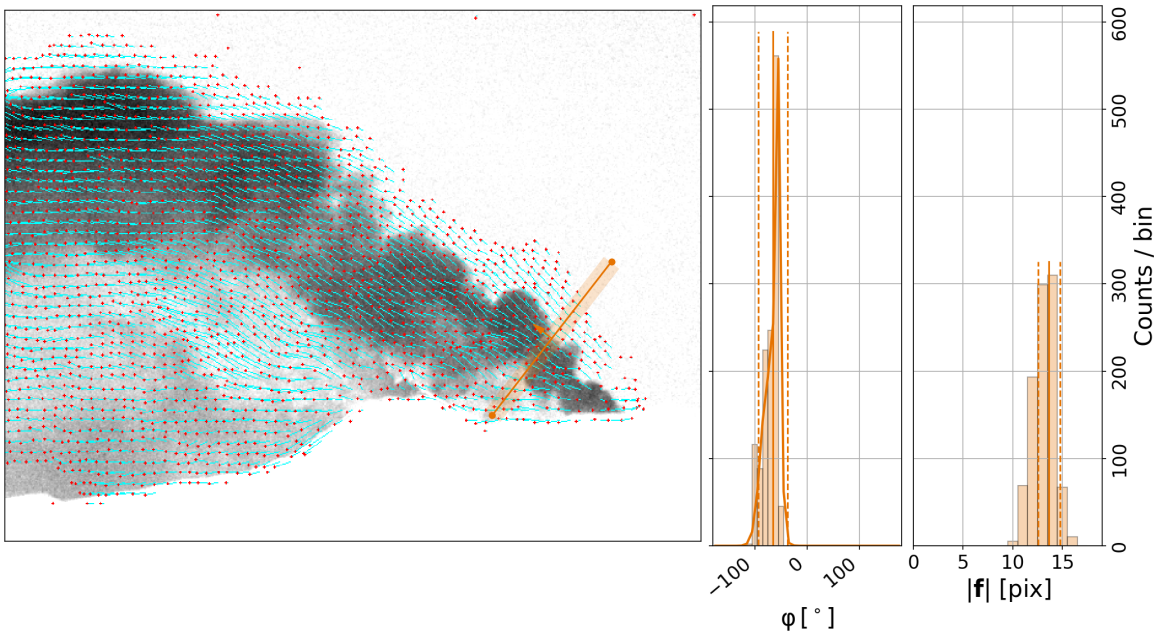

Figure 9. Plume velocity optical flow - Example output of the Farnebäck optical flow algorithm including histograms of the flow vector orientation angles φ (middle) and magnitudes |f| (right) within an example ROI around the indicated PCS line (orange). From the latter, a plume velocity of $4.2\,(\pm 0.4)$ m/s and a predominant movement direction of $\theta = -65\,(\pm 14)\,^\circ$ was retrieved using first and second moments of the displayed histogram distributions.

velocity retrievals, including the histogram post analysis method, are introduced in ex. script 9 (see Table A1).

3.6. Image based signal dilution correction

A correction for the signal dilution effect (see Sect. 2.4) can be performed using the `DilutionCorr` class. The method is based on [19] and uses the model function

$$I_{\text{meas}}(\lambda) = I_0(\lambda)e^{-\epsilon(\lambda)d} + I_A(\lambda)(1 - e^{-\epsilon(\lambda)d}) \tag{5}$$

to retrieve atmospheric extinction coefficients ϵ in the on and off-band regime. Here, I_{meas} are measured intensities of dark terrain features within the images, d is the distance to these features and I_0 their initial intensity. The ambient intensity I_A can be approximated using gas free sky areas in the plume images ([19]). For the retrieval, a set of measured intensities I_{meas} is extracted from vignetting corrected plume images using suitable terrain features (e.g. pixels along a volcanic flank). These intensities are fitted to Eq. 5 (as a function of their distance d) in order to retrieve the extinction coefficients in both wavelength regimes. The required distances d to the features can be retrieved automatically, based on intersections of individual pixel viewing directions with the local topography (using the Geonum library, for details see Appendix A).

The plume images can then be corrected for the signal dilution effect using the retrieved extinction coefficients (see Eq. 4 in [19]). The correction is only applied to plume pixels (e.g. using a τ_{AA} threshold mask). The required plume distances can be retrieved from the measurement geometry (for details see Sect. 3.1).

Figure 10 shows results of an example dilution correction using an on and off-band image from the Etna example data, recorded at 06:45 UTC. Extinction coefficients of $\epsilon_{\text{on}} = 0.0743\,\text{km}^{-1}$ (Figure 10a)

Preprints (www.preprints.org) | NOT PEER-REVIEWED | Posted: 13 October 2017 doi:10.20944/preprints201710.0085.v1

Peer-reviewed version available at Geosciences 2017, 7, 134; doi:10.3390/geosciences7040134

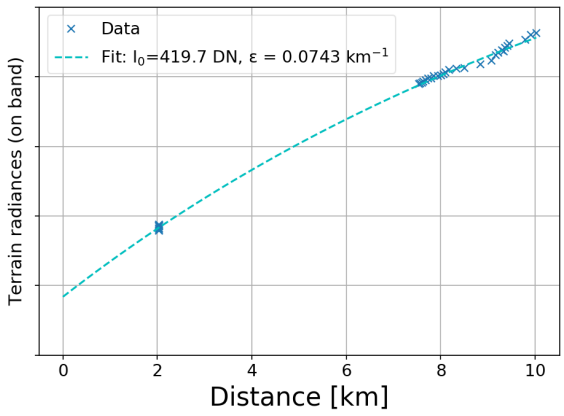

(a) Fit result on-band

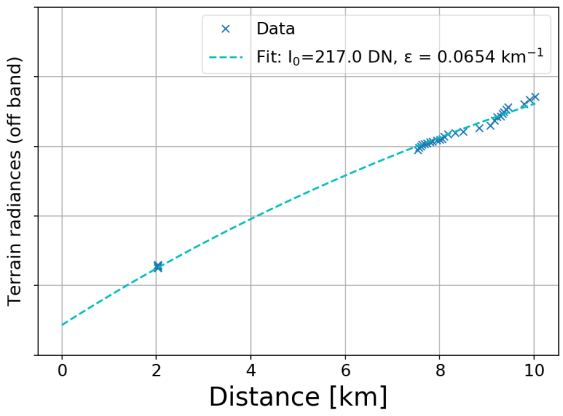

(b) Fit result off-band

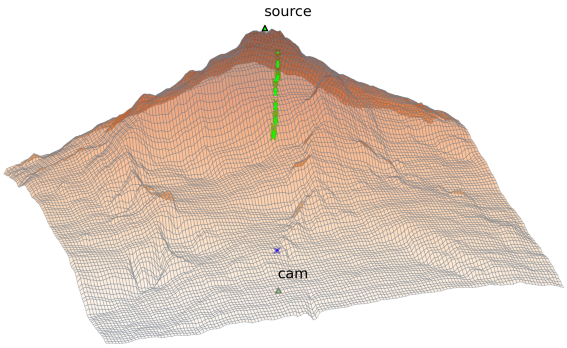

(c) 3D map distance retrieval

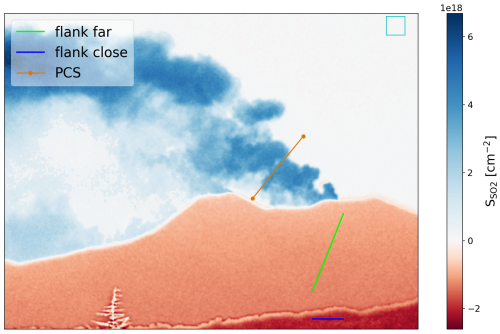

(d) Corrected SO_2-CD image

Figure 10. Signal dilution correction - (a) and (b) show the fit result of an example dilution analysis for the on and off-band regime, respectively. (c) shows a 3D map of the camera scene and (d) a dilution corrected SO_2-CD image. The terrain features used for the dilution analysis are indicated in (c) and (d) (blue and lime coloured lines). (d) further includes the image region used to estimate the ambient intensity I_A (blue rectangle) and an example PCS line used to compare emission-rates before and after the correction.

and $\epsilon_{\text{off}} = 0.0654\,\text{km}^{-1}$ (Figure 10b) were retrieved using the two topographic profile lines shown in Figure 10c and 10d. The correction yields an emission-rate of 4.8 ($\pm$ 1.2) kg/s using the PCS line shown in Figure 10d. The emission-rate of the uncorrected image is 1.6 ($\pm$ 0.8) kg/s, corresponding to an underestimation of approximately 67 % at an average plume distance of 10.4 ($\pm$ 0.1) km.

3.7. Emission-rate retrieval

Emission-rates can be determined using the `EmissionRateAnalysis` class. The analysis is performed based on an image list containing calibrated SO_2-CD images (see also Appendix D.2) and a specification of one or more retrieval PCS lines (`LineOnImage` objects, cf. Figure 2). Plume velocities can be provided by the user (e.g. using the result of a cross-correlation analysis, see Sect. 3.5.1) or can be retrieved automatically during the emission-rate analysis using the Farnebäck optical flow routine (see Sect. 3.5.2). For the latter, three options are available:

1. *flow_raw* $\rightarrow$ the raw output of the Farnebäck algorithm is used. This should only be done if it can be assured that the algorithm yields reliable output in the considered plume area (i.e. ROI around the PCS line) and for all images of the time-series.

Preprints (www.preprints.org) | NOT PEER-REVIEWED | Posted: 13 October 2017 doi:10.20944/preprints201710.0085.v1

Peer-reviewed version available at Geosciences 2017, 7, 134; doi:10.3390/geosciences7040134

2. *flow_histo* → performs the histogram post-analysis proposed by [35] (cf. Sect. 3.5.2). The retrieved local average velocity vector for each PCS line is then used as a velocity estimate for the corresponding retrieval line.
3. *flow_hybrid* → reliable motion vectors from the flow field are used while unreliable ones are identified and replaced based on the histogram post-analysis (see prev. point).

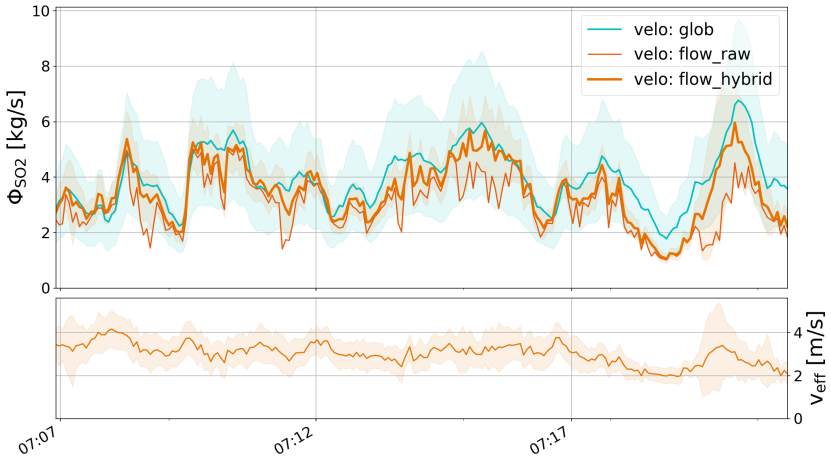

Figure 11. Emission-rate retrieval - Emission-rates (top) and plume velocities (bottom) of the Etna example dataset on 16 September 2015 between 07:06 – 07:22 UTC using the retrieval line "PCS" shown in Figure 8. The analysis was performed using 1.) a global velocity of 3.5 m/s (cyan, velo: glob, from the cross-correlation analysis), 2.) the raw output of the Farnebäck algorithm (thin orange) and 3.) using the *flow_hybrid* method (bold orange). The retrieved effective velocities are plotted in the lower panel and correspond to the average velocities along the PCS line using the *flow_hybrid* method. Uncertainties are displayed as shaded areas.

Figure 11 shows results from an emission-rate analysis for the Etna test data (upper panel) including plume velocities retrieved using the *flow_hybrid* method (lower panel). The AA images were calculated from dilution corrected on and off-band plume images using background modelling mode 6 (cf. Sect. 3.3) and were corrected for cross-detector sensitivity variations using a mask retrieved from cell *"a53"* (cf. Figure 5a). The AA images were calibrated using the *Pearson* DOAS calibration curve shown in Figure 6.

4. Conclusions

In this paper the software package *Pyplis* was introduced. *Pyplis* contains an extensive collection of relevant algorithms for the analysis of UV SO_2 camera data, particularly for the retrieval of emission-rates from SO_2-emitters (e.g. volcanoes, power plants, ships).

Apart from established analysis methods, such as cross-correlation based velocity retrievals (e.g. [26]) or cell and DOAS calibration (e.g. [18]), *Pyplis* incorporates more recent developments. These include an implementation of the DOAS FOV retrieval algorithm proposed by [25], a routine to correct for the signal dilution effect based on [19], or pixel based gas velocity retrievals using an optical flow algorithm (e.g. [20]). The latter incorporates a method to detect and correct for ill-constraint optical flow motion-vectors based on [35]. Furthermore, *Pyplis* includes a framework to perform a detailed 3D-analysis of the observed camera scene including automatic online access to high resolution topography data from the SRTM dataset. This enables, for example, to retrieve the camera viewing direction based on distinct topographic features in the images (e.g. volcano summit), or to calculate distances between the camera and the local topography at a pixel-level. The latter is of particular relevance for the image based correction of the signal dilution effect.

Due to this extensive collection of algorithms, *Pyplis* provides flexibility with regard to the analysis strategy and is highly adaptable to different data situations. The object oriented architecture of the API gives intuitive access to the main features and makes it easy to compare individual methods (e.g. different plume velocity retrievals, as illustrated in this paper). *Pyplis* is open-source and can be operated both on Windows and Unix machines. Thus, it is well suited for inter-comparison studies, the exchange of analysis results or for the development and verification of new methods.

The *Pyplis* installation includes numerous example scripts which were used in this paper to introduce the main features of the software. The examples are based on a 15 min dataset recorded at Mt. Etna, Italy in September 2015 which is freely available and can be downloaded from the website.

Finally, the authors wish to point out that *Pyplis* may also be used for other applications based on the same measurement principle (e.g. NO_2 cameras) and that parts of it can also be useful for other remote sensing applications (e.g. the engine for geometrical calculations). The *Pyplis* software is hosted on GitHub: https://github.com/jgliss/pyplis. The code documentation and further information (e.g. installation instructions) can be found on the documentation website: http://pyplis.readthedocs.io.

Acknowledgments: The authors like to thank the *Atmosphere and Remote Sensing* group from the Institute of Environmental Physics in Heidelberg, Germany for providing image data for test purposes and for collaboration during the Etna field campaign in 2015. The work of K.S., A.K. and A.S.D. was partly supported by the European Research Council (ERC) under the European Union's Horizon 2020 research and innovation programme under grant agreement No 670462 (COMTESSA). J.G. wishes to thank T. Skauli, M. Vogt, and A. Donath for helpful discussions related to the development of the software and the drafting of the manuscript.

Author Contributions: J.G. designed, developed and tested the software including the example scripts and wrote the manuscript. K.S., A.S.D., A.K, H.S. and A.S. contributed to the API design (selection of implemented methods / algorithms) and helped testing and debugging the code. H.S. provided the IFR algorithm and wrote the corresponding part in the paper.

Conflicts of Interest: The authors declare no conflict of interest.

Abbreviations

The following abbreviations are used in this manuscript:

UV	Ultraviolet
CD	Column density
DOAS	Differential optical absorption spectroscopy
FOV	Field of view
OD	Optical density
AA	SO_2 apparent absorbance
PCS	Plume cross section
ICA	Integrated column amount
API	Application programming interface
IFR	In-operation field-of-view retrieval

Appendix A. The Geonum Python library

The *Pyplis* class `MeasGeometry` (see Sect. 3.1) makes use of the Python library Geonum [31]. Geonum was developed by J. Gliss in parallel to *Pyplis* and features vector based geographical calculations in three dimensions as well as access and handling of high resolution topographic data. It supports topographic data based on the Etopo1 global relief model ([36]) and from the NASA shuttle radar topography mission (SRTM, [37]). The latter can be accessed and downloaded automatically within Geonum from the SRTM online database (for details see information on the Geonum [31] website).

Appendix A.1. Pixel based retrieval of distances to local terrain features

Distances to topographic features can be retrieved at the pixel-level based on the camera position and viewing direction by calculating the intersections of individual pixel viewing directions (i.e.

azimuth and elevation angle) with the local topography. This is particularly helpful for the image based correction of the signal dilution effect (see Sect. 3.6 and Figure 10).

Appendix B. Dark and offset correction

Pyplis includes two options to perform dark and offset corrections for image data. Both methods require access to the exposure time of the images (e.g. from the image file names, see also Appendix E).

1. **Option 1: Modelling of dark / offset image**
   The correction is performed based on two dark images, one being recorded at short(est) exposure time (offset signal O) and the second one at long(est) exposure time (dark current + offset signal, D). A dark image is then calculated based on the exposure time of the input image I using the following formula:
   $$D_{\mathrm{mod}} = O + \frac{(D - O) * t_{\mathrm{exp,I}}}{(t_{\mathrm{exp,D}} - t_{\mathrm{exp,O}})}. \quad \text{(A1)}$$
   This mode is, for instance, used for the Envicam-2 camera type (see Appendix E.2). The corresponding method `model_dark_image` is part of the *processing.py* module.

2. **Option 2: Subtraction of dark image**
   Dark and offset correction is performed by subtracting a single dark image D (containing dark and offset) which thus, needs to be recorded at the same camera exposure time. This mode is for instance used for the HD-Custom camera (see Appendix E.2).

The detector dark current depends on the temperature. In case of temperature variations it is therefore recommended to use dark images recorded close in time to a given plume image.

Appendix C. Spectrometer FOV search: additional information

Appendix C.1. Temporal merging of image and DOAS data

The `ImgStack` class includes three methods to merge a set of camera images (stacked within such an `ImgStack`) and a DOAS time series vector, both sampled on arbitrary irregular grids.

- **First method: averaging of camera images**
  This method averages all images in the stack based on start / stop time stamps of the spectrometer data (i.e. the image sampling rate should be larger than the spectrum sampling rate). Spectra for which no image data could be found are removed.

- **Second method: vice versa interpolation of both grids**
  This method uses the unified sampling grid (all time stamps from both datasets) and performs interpolation of the DOAS data vector (at image acquisition time stamps) and vice versa. The method is slow compared to method 1 since each image pixel of the stack is interpolated. However, it results in more data points, which can be an advantage especially for short time series. This method can be significantly accelerated by reducing the image size or by only performing the analysis within a certain image region (c.f. example script no. 6, Table A1, script option: DO_FINE_SEARCH). The time series interpolation is done using the *pandas* Python library.

- **Third method: nearest data point**
  This method loops over all spectra and for each spectrum, finds the image which is nearest in time. This method is for instance used, if only the acquisition time stamps are provided and not the start / stop stamps of each exposure (which is required for the first method).

Peer-reviewed version available at Geosciences 2017, 7, 134; doi:10.3390/geosciences7040134

Appendix C.2. FOV determination applying the IFR method

The In-operation Field of view Retrieval (IFR) method is an implementation of the method proposed by [25]. IFR applies a linear camera model to invert the FOV of a low-resolution instrument (in this case a DOAS spectrometer) from imager data without a-priori information (e. g. FOV position, size and shape). The inversion problem is typically under-determined for SO_2 camera applications. Therefore, the iterative LSMR method ([38]) is applied to retrieve the FOV coefficients depending on the regularisation parameter λ.

The choice of λ is somewhat arbitrary, but may influence the IFR results depending on the input data quality. The default value is $\lambda = 10^{-6}$. However, in case only a small sample size is available, λ may need to be increased (e. g. $\lambda = 10^{-3}$) in order to produce meaningful results. A side effect of increasing λ is a spatial smoothing of the results potentially leading to unrealistic large FOVs. Figure 7b shows a sample FOV distribution retrieved from the Etna test data (88 images) using $\lambda = 2 \cdot 10^{-3}$.

In order to reach the final goal of gaining a calibration curve from the image stack containing AA images, individual images need to be convolved with the FOV of the low-resolution instrument. Therefore, a parametrised FOV is fitted to the IFR results, which is more applicable to ground-based instruments than the parametrisation proposed by [25]. We propose the following elliptical Super-Gaussian FOV parametrisation g of the IFR result depending on pixel coordinates i, j in horizontal and vertical direction, respectively:

$$g(i,j) = C + Ae^{-\left(\left[\frac{i-i_m}{\sigma}\right]^2 + \left[\frac{(j-j_m)a}{\sigma}\right]^2\right)^b} \tag{A2}$$

where, C is a constant offset, A the amplitude, x_m and y_m define the centre position, σ measures the width in x-direction, the asymmetry parameter a measures the ratio of the semi-axes (e.g. $a = 1$ yields an only circular FOV), and b is the shape parameter of the Super Gaussian (e.g. $b = 1$ yields an only Gaussian FOV, $b = 10$ approximates a flat-disk FOV).

If an additional tilt of the FOV is required in case of an elliptical FOV, the above fit may be performed in a transformed coordinate system.

$$\begin{pmatrix} i' \\ j' \end{pmatrix} = \begin{pmatrix} \cos\theta & -\sin\theta \\ \sin\theta & \cos\theta \end{pmatrix} \begin{pmatrix} i - i_m \\ j - j_m \end{pmatrix} \tag{A3}$$

defines the transformation into tilted coordinates i' and j'. Equation (A2) is then replaced by

$$g = C + A \exp\left[-\left(\left[\frac{i'}{\sigma}\right]^2 + \left[\frac{j'a}{\sigma}\right]^2\right)^b\right]. \tag{A4}$$

Appendix D. Basic data structure

The *Pyplis* code hierarchy for the emission-rate analysis is shown in Figure 2. The structure is based on the work flow shown in Figure A1 and includes most of the relevant classes required for the emission-rate analysis.

Appendix D.1. Setup and Dataset classes

The most important classes related to data import and image management are:

- Setup classes (e.g. `Camera`, `Source`, `MeasSetup`), which can be used to specify all relevant meta information.
- Dataset classes (`Dataset`, `CellCalibEngine`), which can be used for automatic image separation, for instance by image type (e.g. on, off, dark, offset) or acquisition time.

Preprints (www.preprints.org) | NOT PEER-REVIEWED | Posted: 13 October 2017 doi:10.20944/preprints201710.0085.v1

Peer-reviewed version available at Geosciences 2017, 7, 134; doi:10.3390/geosciences7040134

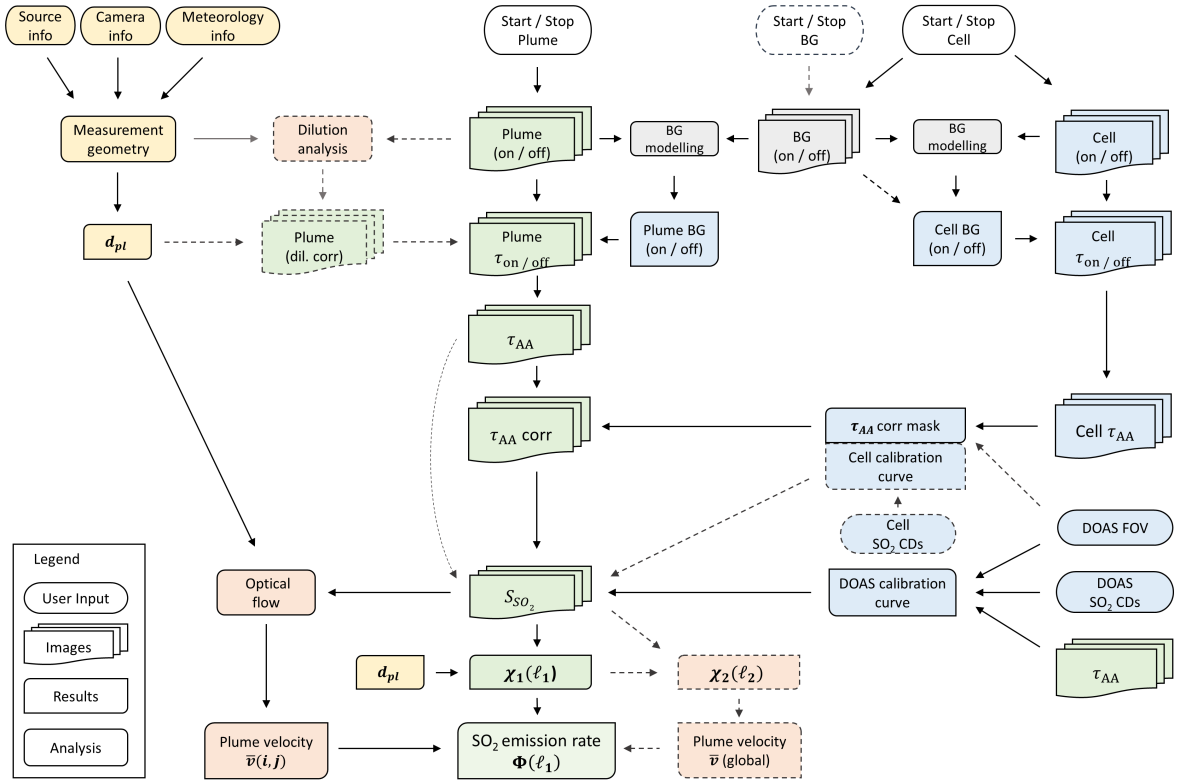

Figure A1. Main analysis steps - Flowchart showing the main analysis steps for emission-rate retrievals (cf. Table 1). The colours indicate geometrical calculations (yellow), background modelling (light gray), camera calibration (light blue), plume speed retrieval (light orange) and the central processing steps for the emission-rate retrieval (light green). Shaded and dashed symbols indicate optional or alternative analysis methods.

Appendix D.2. ImgList classes

Image list classes are central for the data analysis. They can be found in the *imagelists.py* module (e.g. `ImgList`, `CellImgList`). An `ImgList` typically contains images of one specific type (e.g. on-band) corresponding to a certain time window. In order to avoid potential memory overflows, images are loaded, processed and unloaded successively within `ImgList` objects. The most important features are described in the following.

Linking of `ImgList` objects

`ImgList` can be linked to each other (e.g. off to on-band list). This means, that, whenever the list index (i.e. the current image) is changed in `ImgList` *A* (e.g. the on-band images), it is also changed in `ImgList` *B* (if *B* is linked to *A*), such that the current image in *B* is closest in time to the one in *A*.

Image preparation and processing modes

Image lists include several image preparation options (e.g. size reduction, cropping, blurring). Further, if certain requirements are fulfilled, additional preparation options and routines can be activated:

- ***darkcorr_mode*** → images are automatically corrected for dark and offset. Requires a dark image (or an `ImgList` containing dark images) to be available in the list. For dark correction mode 1 (see appendix B), also an offset image (or list) must be available.

Preprints (www.preprints.org) | NOT PEER-REVIEWED | Posted: 13 October 2017 doi:10.20944/preprints201710.0085.v1

Peer-reviewed version available at Geosciences 2017, 7, 134; doi:10.3390/geosciences7040134

- ***tau_mode*** → if active, images are converted into τ images on image load (using the `PlumeBackgroundModel` class to retrieve the plume background intensities). Requires availability of a sky reference image in the list (only for background modelling modes 1 - 6, see Sect. 3.3).
- ***aa_mode*** → if active, images are converted into τ_{AA} images on image load. Requires an off-band image list to be linked to the list and availability of a sky reference image in both lists (only for background modelling modes 1 - 6, see Sect. 3.3).
- ***sensitivity_corr_mode*** → if active, images will be corrected for sensitivity variations due to shifts in the filter transmission windows (see Sect. 2.2). Requires a corresponding correction mask to be available in the list. The latter can for instance be retrieved from cell calibration data (see Sect. 3.4.1).
- ***calib_mode*** → images are loaded as calibrated SO_2-CD images. Requires list to be in *aa_mode* and calibration data to be available in the list. The latter can be of type `CellCalibData` or `DoasCalibData` (see Figure 2). Warns if *sensitivity_corr_mode* is inactive.
- ***optflow_mode*** → if active, the Farnebäck optical flow will be calculated between current and the next list image (using the `OptflowFarneback` class, see Sect. 3.5.2).
- ***vigncorr_mode*** → if active, images will be corrected for vignetting. Requires availability of a vignetting mask in the list or a sky reference image from which the mask is determined.

All active image preparation options are applied on image load (i.e. whenever the current image is changed in the `ImgList`).

Appendix D.3. Processing classes

Most of the relevant processing classes are shown in Figure 2. They include:

- `MeasGeometry` (*geometry.py*) → all relevant geometrical calculations (Sect. 3.1).
- `OptflowFarneback` (*plumespeed.py*) → calculation and post analysis of optical flow field between two images (Sect. 3.5.2).
- `CellCalibData` (*cellcalib.py*) → pixel based retrieval of cell calibration polynomial (based on a set of cell τ images) and retrieval of sensitivity correction mask (Sect. 3.4.1).
- `DoasFovEngine`(*doascalib.py*) → performs FOV search of DOAS spectrometer within camera images (Sects. 3.4.2 & C).
- `DoasFov` (*doascalib.py*) → DOAS FOV information such as position, shape, convolution mask (Sects. 3.4.2 & C). Can be saved as FITS file.
- `DoasCalibData` (*doascalib.py*) → DOAS calibration data, i.e. vector of τ and SO_2-CD values for fitting of calibration polynomial (Sect. 3.4.2). Can be saved as FITS file.
- `LineOnImage` (*processing.py*) → data extraction (interpolation) along a line on a discrete 2D image grid (e.g. SO_2-CDs from calibrated images or displacement vectors from optical flow field, Sect. 3.7).
- `EmissionRateAnalysis` (*fluxcalc.py*) → Performs emission-rate analysis based on an `ImgList` containing calibrated images. Emission-rates can be retrieved along one (or more) plume cross section lines (`LineOnImage` objects). Has several options related to the plume velocity retrieval (Sect. 3.7).
- `EmissionRates` (*fluxcalc.py*) → Contains results (time series) of an emission-rate analysis (i.e. including plume velocity data). Specific for one PCS line and one velocity retrieval (e.g. the analysis shown in Figure 11 creates 3 `EmissionRates` objects for each of the 3 different velocity retrievals, Sect. 3.7).

Further important classes (not shown in Figure 2) are:

- `PlumeBackgroundModel` (*plumebackground.py*) → performs τ image modelling using either of the available modelling modes (Sect. 3.3).
- `VeloCrossCorrEngine` (*plumespeed.py*) → high level class to calculate the plume velocity using the cross-correlation method (Sect. 3.5.1).

Preprints (www.preprints.org) | NOT PEER-REVIEWED | Posted: 13 October 2017 doi:10.20944/preprints201710.0085.v1

Peer-reviewed version available at Geosciences 2017, 7, 134; doi:10.3390/geosciences7040134

- `DilutionCorr` (*dilutioncorr.py*) → engine to perform signal dilution correction (Sect. 3.6).
- `ImgStack` (*processing.py*) → contains a series of images (stored as 3D numpy array) as well as supplementary data (e.g. acq. time stamps, exposure times of all stacked images) and basic processing operations (time merging with other data, up / downscaling). Can be saved as FITS file.

Appendix E. Supplementary information and test data

Appendix E.1. Example dataset and example scripts

Most of the example and introduction scripts provided with *Pyplis* are based on a short example dataset recorded at Mt. Etna, Italy on 16.09.2015, using a type Envicam-2 camera. It includes ∼ 15 minutes of plume data (between 07:06 – 07:22 UTC, see e.g. Figure 11.) as well as cell calibration data including suitable background images (between 06:59 – 07:04 UTC, see Figure 5). These data is used for demonstration purposes in the provided example scripts, which are summarised in Table A1. The data is not part of the *Pyplis* installation and can be downloaded from the website.

Table A1. *Pyplis* example scripts, sub-categorised into introductory scripts (0.1–0.7) and scripts related to the emission-rate analysis of the Etna test data (1–12)

No.	Name	Description	Sect
0.1	ex0_1_img_handling.py	The `Img` class - Image import and dark correction	3.2
0.2	ex0_2_camera_setup.py	The `Camera` class - Definition of camera specifications and image file name convention	D
0.3	ex0_3_imglists_manually.py	Introduction into `ImgList` objects	D.2
0.4	ex0_4_imglists_auto.py	Automatic creation of `ImgList` objects using the ECII default `Camera` type	D.2
0.5	ex0_5_optflow_livecam.py	Interactive optical flow using web cam	3.5.2
0.6	ex0_6_pcs_lines.py	Plume cross section lines (creation and orientation of `LineOnImage` objects)	3.7
0.7	ex0_7_cellcalib_manual.py	Introduction into cell calibration and the `CellCalibData` object (manually)	3.4.1
1	ex01_analysis_setup.py	Create `MeasSetup` class and initiate analysis `Dataset` object from that (see Figure 2)	3.4.1
2	ex02_meas_geometry.py	Introduction into the `MeasGeometry` class	3.1
3	ex03_plume_background.py	The `PlumeBackgroundModel` class - background modelling and τ image retrieval	3.3
4	ex04_prep_aa_imglist.py	Preparation of image list containing AA images	D.2
5	ex05_cell_calib_auto.py	Automatic cell calibration using the `CellCalibEngine` class	3.4.1
6	ex06_doas_calib.py	DOAS calibration and FOV search	3.4.2
7	ex07_doas_cell_calib.py	Retrieval of AA sensitivity correction mask	3.4
8	ex08_velo_crosscorr.py	Plume velocity retrieval using cross-correlation	3.5.1

9	ex09_velo_optflow.py	Plume velocity retrieval using Farnebäck optical flow algorithm using `OptflowFarneback` class	3.5.2
10	ex10_bg_imglists.py	Retrieval of background image lists (on, off) using `Dataset` class	D
11	ex11_signal_dilution.py	Correction for signal dilution and the `DilutionCorr` class	3.6
12	ex12_emission_rate.py	Emission-rate retrieval for the test dataset	3.7
	SETTINGS.py	Global settings for example scripts	

Appendix E.2. Camera specifications

In order to use all features of *Pyplis* (e.g. automatic file separation, automatic dark and offset correction, geometrical calculations), certain camera characteristics need to be provided by the user. These information is typically specified within a `Camera` class (*setupclasses.py* module). The required information includes specifications about the image sensor (e.g. pixel geometry) and optics (e.g. focal length) as well as file naming conventions (e.g. how to retrieve the filter type or the image acquisition time from file names). *Pyplis* provides the possibility to define new default camera types which store all relevant camera information to the *Pyplis* data file *cam_info.txt*, which can be found in the *data* directory of the installation (see ex. script 0.2 for details).

Appendix E.3. Source specifications

Default source information (e.g. longitude, latitude, altitude) can be specified in the file *my_sources.txt* in the installation *data* directory.

References

1. Robock, A. Volcanic eruptions and climate. *Reviews of Geophysics* **2000**, *38*, 191–219.
2. IPCC. *Climate Change 2013: The Physical Science Basis. Contribution of Working Group I to the Fifth Assessment Report of the Intergovernmental Panel on Climate Change*; Cambridge University Press: Cambridge, United Kingdom and New York, NY, USA, 2013; p. 1535.
3. Carroll, M.R.; Holloway, J.R. *Volatiles in magmas*; Mineralogical Society of America, 1994. Last access: 30 July 2017.
4. Oppenheimer, C.; Fischer, T.; Scaillet, B. 4.4 - Volcanic Degassing: Process and Impact. In *Treatise on Geochemistry (Second Edition)*; Elsevier, 2014; pp. 111–179.
5. Lübcke, P.; Bobrowski, N.; Arellano, S.; Galle, B.; Garzón, G.; Vogel, L.; Platt, U. BrO / SO_2 molar ratios from scanning DOAS measurements in the NOVAC network. *Solid Earth* **2014**, *5*, 409–424.
6. Bobrowski, N.; von Glasow, R.; Giuffrida, G.B.; Tedesco, D.; Aiuppa, A.; Yalire, M.; Arellano, S.; Johansson, M.; Galle, B. Gas emission strength and evolution of the molar ratio of BrO / SO_2 in the plume of Nyiragongo in comparison to Etna. *Journal of Geophysical Research: Atmospheres* **2015**, *120*, 277–291. 2013JD021069.
7. Moffat, A.J.; Millan, M.M. The applications of optical correlation techniques to the remote sensing of SO_2 plumes using sky light. *Atmospheric Environment (1967)* **1971**, *5*, 677–690.
8. Platt, U.; Stutz, J. *Differential Optical Absorption Spectroscopy: Principles and Application*; Springer, 2008.
9. Platt, U.; Perner, D. Direct measurements of atmospheric CH_2O, HNO_2, O_3, NO_2, and SO_2 by differential optical absorption in the near UV. *J. Geophys. Res.* **1980**, *85*, 7453–7458.
10. Galle, B.; Johansson, M.; Rivera, C.; Zhang, Y.; Kihlman, M.; Kern, C.; Lehmann, T.; Platt, U.; Arellano, S.; Hidalgo, S. Network for Observation of Volcanic and Atmospheric Change (NOVAC) - A global network for volcanic gas monitoring: Network layout and instrument description. *J. Geophys. Res.* **2010**, *115*.
11. Mori, T.; Burton, M. The SO_2 camera: A simple, fast and cheap method for ground-based imaging of SO_2 in volcanic plumes. *Geophysical Research Letters* **2006**, *33*.

12. Bluth, G.; Shannon, J.; Watson, I.; Prata, A.; Realmuto, V. Development of an ultra-violet digital camera for volcanic SO_2 imaging. *Journal of Volcanology and Geothermal Research* **2007**, *161*, 47 – 56.
13. Kantzas, E.P.; McGonigle, A.; Tamburello, G.; Aiuppa, A.; Bryant, R.G. Protocols for UV camera volcanic SO2 measurements. *Journal of Volcanology and Geothermal Research* **2010**, *194*, 55 – 60.
14. Stebel, K.; Amigo, A.; Thomas, H.; Prata, A. First estimates of fumarolic SO_2 fluxes from Putana volcano, Chile, using an ultraviolet imaging camera. *Journal of Volcanology and Geothermal Research* **2015**, *300*, 112–120.
15. D'Aleo, R.; Bitetto, M.; Delle Donne, D.; Tamburello, G.; Battaglia, A.; Coltelli, M.; Patanè, D.; Prestifilippo, M.; Sciotto, M.; Aiuppa, A. Spatially resolved SO_2 flux emissions from Mt Etna. *Geophys. Res. Lett.* **2016**, *43*, 7511–7519.
16. Tamburello, G.; Aiuppa, A.; McGonigle, A.J.S.; Allard, P.; Cannata, A.; Giudice, G.; Kantzas, E.P.; Pering, T.D. Periodic volcanic degassing behavior: The Mount Etna example. *Geophys. Res. Lett.* **2013**, *40*, 4818–4822.
17. Kern, C.; Kick, F.; Lübcke, P.; Vogel, L.; Wöhrbach, M.; Platt, U. Theoretical description of functionality, applications, and limitations of SO_2 cameras for the remote sensing of volcanic plumes. *Atmospheric Measurement Techniques* **2010**, *3*, 733–749.
18. Lübcke, P.; Bobrowski, N.; Illing, S.; Kern, C.; Alvarez Nieves, J.M.; Vogel, L.; Zielcke, J.; Delgado Granados, H.; Platt, U. On the absolute calibration of SO_2 cameras. *Atmospheric Measurement Techniques* **2013**, *6*, 677–696.
19. Campion, R.; Delgado-Granados, H.; Mori, T. Image-based correction of the light dilution effect for SO_2 camera measurements. *Journal of Volcanology and Geothermal Research* **2015**, *300*, 48 – 57.
20. Peters, N.; Hoffmann, A.; Barnie, T.; Herzog, M.; Oppenheimer, C. Use of motion estimation algorithms for improved flux measurements using SO_2 cameras. *Journal of Volcanology and Geothermal Research* **2015**, *300*, 58 –69.
21. Kern, C.; Lübcke, P.; Bobrowski, N.; Campion, R.; Mori, T.; Smekens, J.F.; Stebel, K.; Tamburello, G.; Burton, M.; Platt, U.; Prata, F. Intercomparison of SO_2 camera systems for imaging volcanic gas plumes. *Journal of Volcanology and Geothermal Research* **2015**, *300*, 22–36.
22. Tamburello, G.; Kantzas, E.; McGonigle, A.; Aiuppa, A. Vulcamera: a program for measuring volcanic SO_2 using UV cameras. *Annals of Geophysics* **2011**, *54*.
23. Peters, N. Plumetrack SO_2 flux calculator. https://ccpforge.cse.rl.ac.uk/gf/project/plumetrack/, 2014. (accessed: 11.09.2017).
24. Kern, C.; Sutton, J.; Elias, T.; Lee, L.; Kamibayashi, K.; Antolik, L.; Werner, C. An automated SO_2 camera system for continuous, real-time monitoring of gas emissions from Kīlauea Volcano's summit Overlook Crater. *Journal of Volcanology and Geothermal Research* **2015**, *300*, 81–94.
25. Sihler, H.; Lübcke, P.; Lang, R.; Beirle, S.; de Graaf, M.; Hörmann, C.; Lampel, J.; Penning de Vries, M.; Remmers, J.; Trollope, E.; Wang, Y.; Wagner, T. In-operation field-of-view retrieval (IFR) for satellite and ground-based DOAS-type instruments applying coincident high-resolution imager data. *Atmospheric Measurement Techniques* **2017**, *10*, 881–903.
26. McGonigle, A.J.S.; Hilton, D.R.; Fischer, T.P.; Oppenheimer, C. Plume velocity determination for volcanic SO_2 flux measurements. *Geophysical Research Letters* **2005**, *32*. L11302.
27. Klein, A.; Lübcke, P.; Bobrowski, N.; Kuhn, J.; Platt, U. Plume propagation direction determination with SO_2 cameras. *Atmospheric Measurement Techniques* **2017**, *10*, 979–987.
28. Kern, C.; Deutschmann, T.; Vogel, L.; Wöhrbach, M.; Wagner, T.; Platt, U. Radiative transfer corrections for accurate spectroscopic measurements of volcanic gas emissions. *B. Volcanol.* **2010**, *72*, 233–247.
29. Kern, C.; Deutschmann, T.; Werner, C.; Sutton, A.J.; Elias, T.; Kelly, P.J. Improving the accuracy of SO_2 column densities and emission rates obtained from upward-looking UV-spectroscopic measurements of volcanic plumes by taking realistic radiative transfer into account. *Journal of Geophysical Research: Atmospheres* **2012**, *117*.
30. Vogel, L.; Galle, B.; Kern, C.; Delgado Granados, H.; Conde, V.; Norman, P.; Arellano, S.; Landgren, O.; Lübcke, P.; Alvarez Nieves, J.M.; Cárdenas Gonzáles, L.; Platt, U. Early in-flight detection of SO_2 via Differential Optical Absorption Spectroscopy: a feasible aviation safety measure to prevent potential encounters with volcanic plumes. *Atmospheric Measurement Techniques* **2011**, *4*, 1785–1804.
31. Gliß, J. Geonum. https://github.com/jgliss/geonum, 2016. (accessed: 11.09.2017).
32. Kraus, S. DOASIS: A framework design for DOAS. PhD thesis, 2006. Ph.D. Thesis.

33. Farnebäck, G., Two-Frame Motion Estimation Based on Polynomial Expansion. In *Image Analysis: 13th Scandinavian Conference, SCIA 2003 Halmstad, Sweden, June 29 – July 2, 2003 Proceedings*; Springer Berlin Heidelberg: Berlin, Heidelberg, 2003; pp. 363–370.
34. Bradski, G. The OpenCV Library. *Dr. Dobb's Journal of Software Tools* **2000**.
35. Gliß, J.; Stebel, K.; Kylling, A.; Sudbø, A. Optical flow gas velocity analysis in plumes using UV cameras – Implications for SO_2-emission-rate retrievals investigated at Mt. Etna, Italy, and Guallatiri, Chile. *Atmospheric Measurement Techniques Discussions* **2017**, *2017*, 1–30.
36. Amante, C.; Eakins, B.W. ETOPO1 Global Relief Model converted to PanMap layer format, 2009.
37. Farr, T.G.; Rosen, P.A.; Caro, E.; Crippen, R.; Duren, R.; Hensley, S.; Kobrick, M.; Paller, M.; Rodriguez, E.; Roth, L.; Seal, D.; Shaffer, S.; Shimada, J.; Umland, J.; Werner, M.; Oskin, M.; Burbank, D.; Alsdorf, D. The Shuttle Radar Topography Mission. *Rev. Geophys.* **2007**, *45*.
38. Fong, D.C.L.; Saunders, M. LSMR: An Iterative Algorithm for Sparse Least-Squares Problems. *SIAM Journal on Scientific Computing* **2011**, *33*, 2950–2971.

Sample Availability: The *Pyplis* software is freely available, including the example data and scripts. For more information see http://pyplis.readthedocs.io.